Human Factors in Design, Engineering, and Computing, Vol. 238, 2026, 1888–1898
https://doi.org/10.54941/ahfe1008417

Distance-Dependent Robustness of WiFi CSI-Based Movement Detection Under Outdoor LoS and NLoS Conditions

Prasanta Kr Sen, Mrigank Sharad, and Ram Babu Roy

Rajendra Mishra School of Engineering Entrepreneurship, IIT Kharagpur, Kharagpur, India

ABSTRACT

Device-free Wi-Fi Channel State Information (CSI) sensing offers infrastructure-free motion detection for outdoor security applications such as agricultural perimeter monitoring, yet nearly all published systems are validated indoors under line-of-sight (LoS) and weather-controlled conditions, leaving the performance under non-line-of-sight (NLoS) conditions with vegetation-induced clutter and path offset unquantified. This gap matters because agricultural deployments routinely introduce lateral obstructions — tree canopies, crop rows, and irregular sightlines — that alter CSI signal structure in ways LoS-trained detectors cannot anticipate, making field-ready deployment guidelines essential rather than optional. We tested two detectors — short-time standard deviation (SD) and short-time Fourier transform (STFT)-based Doppler energy — using an ESP32 CSI platform (2.4 GHz, ~100 Hz) across a mango orchard (1–2 m tree spacing) and an open bare field, at NLoS offsets of 0.5–1.5 m, 1.5–2.5 m, and 2.5–3.5 m, against slow/normal/fast LoS baselines. The SD detector collapsed under NLoS attenuation, converging toward the fast-LoS baseline and losing threshold separability beyond 1.5 m, with F1 falling from 0.78 to 0.40 in the orchard and to zero in the open field, whereas Doppler energy remained compact and separable, sustaining F1 of 0.66–0.77 across all open-field distances and degrading more gracefully under vegetation. These results establish a 0.5–1.5 m NLoS reliability boundary for variance-based sensing. Critically, the two environments failed in opposite directions — the orchard degraded SD gradually through attenuation, while the open field caused abrupt threshold collapse — indicating that NLoS-robust CSI sensing requires Doppler-domain features whose reliability depends on scene geometry, not distance alone.

Keywords: ESP32, Wi-Fi CSI, NLoS, STFT-doppler, SD-threshold, Movement detection, Outdoor sensing

INTRODUCTION

Wi-Fi sensing systems built on Channel State Information (CSI) are validated almost exclusively under controlled indoor line-of-sight (LoS) conditions. Yet, smart-farming deployments increasingly place standard 802.11 access points in agricultural and peri-urban settings where the propagation path is rarely clear. CSI extracted from commodity Wi-Fi chipsets encodes multipath effects across all OFDM subcarriers, offering a substantially richer motion-perturbation signature than scalar RSSI, which prior work has shown to be too coarse to resolve subtle movement (Halperin *et al.*, 2011; Wang *et al.*, 2015).

Received September 25, 2026; Revised October 26, 2026; Accepted November 2, 2026; Available online December 1, 2026

© 2026 The Authors. This work is licensed under a Creative Commons Attribution-NonCommercial-NoDerivatives 4.0 License.
For more information, see https://creativecommons.org/licenses/by-nc-nd/4.0/

This makes CSI a candidate for contactless security applications, such as detecting unauthorised human presence, wildlife intrusion, or unattended access events in cultivated fields.

These scenarios routinely place the subject off the direct transmitter-receiver axis, obstructed by vegetation, terrain, or structures—a non-line-of-sight (NLoS) geometry that alters the channel response in ways indoor-trained detectors are not built to handle. Existing NLoS work has concentrated on through-wall sensing at fixed, short ranges (Li *et al.*, 2020), and the broader shift toward deep-learning CSI classifiers has likewise been validated only indoors. A systematic characterisation of detection performance as a function of lateral obstruction distance in outdoor environments with heterogeneous scattering, such as vegetated agricultural fields, is lacking in the literature. We restrict our comparison to two threshold-based detectors rather than learned classifiers because the target platform, an ESP32 CSI node, is intended for low-power field deployment, where a trained model is not always a practical baseline.

From a human-factors perspective, this design choice carries a further consequence: in automated monitoring, miss-prone failures impose a distinct cost relative to false-alarm-prone failures. Operators calibrate trust and reliance on observed error patterns, and systems that fail silently—raising no false alarms while missing a growing share of true events—are particularly prone to inducing misplaced confidence (Raja and Riley, 1997; Lee and See, 2004). This motivates evaluating not only whether detection degrades under NLoS offset, but which failure mode dominates, since the two carry asymmetric consequences for operator reliance in a deployed security system, directly bearing on the reliability and trustworthiness of ambient sensing as a human-centred automation technology.

This paper makes three contributions:

1. The first outdoor, NLoS distance-stratified evaluation of CSI-based motion detection, spanning lateral obstruction offsets of 0.5–3.5 m across three 1-m zones in two environments—a mango orchard and an open bare field—providing reproducible field-deployment benchmarks.
2. A quantitative comparison of two operationally distinct detection paradigms, short-time standard deviation (SD) thresholding and STFT-Doppler energy thresholding, under matched NLoS conditions, showing that their failure modes differ by environment rather than distance alone.
3. Quantification of transient signal features—peak Doppler energy and peak short-time SD—as a function of NLoS zone, establishing attenuation magnitude and its relationship to threshold-crossing probability.

The remainder of the paper is organized as follows. Section 2 reviews CSI-based motion sensing, NLoS propagation effects, and outdoor RF sensing. Section 3 describes the system architecture and both detection algorithms. Section 4 details the data collection protocol and experimental sites. Section 5 presents results with reference to experimental figures. Section 6 concludes with limitations and future work.

RELATED WORK

The foundational insight behind CSI-based sensing—that human motion measurably perturbs the multipath channel across OFDM subcarriers—was formalised by (Halperin *et al.*, 2011) and operationalised through the Intel 5300 CSI tool. (Wang *et al.*, 2017) showed that PCA-based subspace projection of multi-subcarrier CSI amplitude sequences separates activity-specific spectral features with sufficient discriminability for activity recognition, while a related line of work applied similar CSI features to fall detection (Wang, Wu and Ni, 2017; Hu *et al.*, 2022). This body of work extends to gesture recognition, breathing monitoring, and crowd counting, almost entirely under indoor, controlled, LoS conditions.

Threshold-based detectors, the simplest operationally deployable class, compute a scalar summary statistic over a rolling CSI window and compare it against a pre-calibrated boundary. Variance and standard deviation metrics dominate this class due to their low computational cost on microcontroller hardware. Their core assumption—that the statistical distribution of motion-induced CSI perturbation is stationary across environments—is what this work tests directly, and finds to be false.

Frequency-domain approaches using short-time Fourier transform (STFT) extract Doppler signatures of limb motion, which appear as spectral energy in the 0.5–5 Hz band tied to walking cadence (Abdelnasser, Harras and Youssef, 2015; Zhang *et al.*, 2018). These methods incur a higher computational cost but relate more directly to motion kinematics, making them more likely to remain robust to propagation-environment variability. Through-wall sensing, the extreme NLoS case, has been studied at fixed, short transmitter–receiver separations (Li *et al.*, 2020); such work confirms that sufficient energy propagates through construction materials for coarse presence detection, but does not address the variable-offset lateral NLoS geometry characteristic of agricultural deployment. Vegetation propagation loss at 2.4 GHz follows the modified exponential decay model in ITU-R P.833 (ITU, 2016), predicting 3–8 dB of loss per meter through a moderate-leaf-area-index canopy, such as a mango tree canopy. This model captures only power attenuation; it does not describe the structural change in CSI that drives SD-threshold failure—specifically, the redistribution of energy across principal component analysis (PCA) modes and the suppression of short-time variance.

A recent cluster of deep-learning NLoS detectors (Table 1)—spanning DFNN, RNN, CNN, and LSTM-based classifiers, adversarial feature fusion, and PSO-SVM optimisation—reports strong indoor results but shares two limitations relevant here: all are validated indoors, and NLoS is treated as a binary condition rather than a distance-parameterised variable. None reports detection performance as a function of lateral obstruction distance, and none operates in a scattering-rich outdoor environment.

The ESP32 platform, via the esp-csi library, has become the default low-cost hardware for CSI research, enabling extraction of 52-subcarrier data at up to 100 Hz (Gringoli *et al.*, 2019). Outdoor use of this platform remains rare, with most published ESP32 CSI studies confined to laboratory settings. This work supplies the outdoor, distance-stratified evaluation that the ESP32 CSI literature currently lacks.

Table 1: Compare some latest NLoS based Wi-Fi CSI movement detection.

Author(s)	Setting	LoS / NLoS Condition	Environment Type	Detection / Localization Method	NLoS Distance / Range
(Olejniczak *et al.*, 2024)	Indoor	Both	Classroom, office, corridor	DFNN (Deep Feedforward Neural Network)	Not specified
(Zhang *et al.*, 2022)	Indoor	NLoS focus	office spaces	AoA, AoD, ToF, DFS, attenuation	Without direct path:
(Abuhoureyah, Wong and Mohd Isira, 2024)	Indoor	NLoS (through-wall)	Indoor office	RNN-LSTM for HAR; amplitude-based deep learning	Through-wall: not quantified in distance
(Wei *et al.*, 2025)	Indoor	NLoS focus	Indoor	Joint feature fusion, adversarial training; deep CNN	Not specified
(Li *et al.*, 2025)	Indoor	NLOS focus	Office, corridor	PSO-SVM-RBF optimization	Not specified
This work	Outdoor	NLoS (lateral)	Orchard + Bare field	SD + STFT-Doppler	0.5–3.5 m, variable

ALGORITHMIC FORMULATION AND SIGNAL PROCESSING PIPELINE

The CSI acquisition platform uses a pair of ESP32 development boards with PCB antennas operating on IEEE 802.11n at 2.4 GHz, 20 MHz channel width, yielding CSI amplitude across 52 OFDM subcarriers at approximately 100 Hz. This sampling rate provides a 10–20× margin over the Nyquist requirement for human limb Doppler frequencies, which typically fall within 1–5 Hz (Liu *et al.*, 2005). The transmitter broadcasts periodic 802.11 frames; the receiver extracts per-packet CSI and logs the 52-element complex amplitude vector at each epoch. Raw sequences are segmented into fixed windows of length 100 samples (≈1 s) with 75% overlap for feature extraction.

SD-Threshold Detection

For a rolling window of length W samples, short-time standard deviation $\sigma(t)$ is computed over the mean subcarrier-averaged CSI amplitude $|H(t)|$:

$$\sigma(t) = \sqrt{\left(\frac{1}{W} \times \sum_i (|H(t-i)| - \mu)^2\right)}$$

where μ is the window mean. Motion is declared when $\sigma(t)$ exceeds a fixed threshold τ_{SD}, where τ_{SD} calibrated from LoS data. A segment is labelled

"Motion" if at least one threshold-crossing occurs within the window; peak short-time SD per segment is used as the primary transient feature.

STFT-Doppler Detection

The STFT-Doppler method operates in the frequency domain. The processing chain is as follows:

1. Per-subcarrier EWMA (Exponentially Weighted Moving Average) background subtraction with smoothing parameter $\alpha = 0.01$, followed by cross-subcarrier mean subtraction for common-mode rejection.
2. The 52-subcarrier CSI matrix is projected onto its first principal component (PC1).
3. STFT is applied to the PC1 series using a Hann window of length $N_{fft} = 128$ with 75% overlap.
4. Spectral energy is integrated over $[f_{low}, f_{high}] = [0.5\ 5]$ Hz to yield $E_{Doppler}$ per segment.
5. Motion is declared when $E_{Doppler}$ exceeds τ_{STFT}, calibrated from LoS data.

Performance Evaluation

Each trial produces both Motion and No-Motion prediction. Accuracy, sensitivity (TPR), specificity (TNR), and F1-score are reported per the standard confusion-matrix definitions.:

Metric	Formula	Interpretation in this Context
Accuracy	(TP+TN)/(TP+TN+FP+FN)	Overall correctness
Sensitivity (TPR)	TP/(TP+FN)	Proportion of true motions detected
Specificity (TNR)	TN/(TN+FP)	Proportion of true non-motions correctly classified
F1-Score	2·TP/(2·TP+FP+FN)	Harmonic mean balancing precision and recall

EXPERIMENTAL SITES AND DATASET PROTOCOL

Site 1—Horticulture Field (Mango Orchard), IIT Kharagpur: mature mango trees spaced 1–2 m apart along the Tx-Rx path block direct LoS, producing NLoS via absorption, diffraction, and dynamic foliage scattering. Human subjects were positioned at different lateral offsets from the LoS path.
Site 2—Nalanda Ground (Open Area), IIT Kharagpur: a low-clutter baseline with a clear Tx-Rx path; a paved road and bare field sit 5–7 m away, introducing ground-reflection multipath and transient clutter from vehicle or pedestrian traffic.

Platform:	**ESP32 Pair, 2.4 GHz, ~100 Hz, 52 Subcarriers.**
Tx-Rx Separation:	10 m
Participant:	1
LoS Movement:	Upright walking on a fixed trajectory at three speed categories—Slow (≤ 2 km/h), Normal (3–5 km/h), Fast (≥6 km/h)
NLoS Offsets:	0.5–3.5 m at 1 m increments, aggregated into three zones—0.5–1.5 m, 1.5–2.5 m, 2.5–3.5 m.
Segmentation:	Window length 128, 75% overlap
Motion Collected:	41 (Horticulture field), 69 (Nalanda open ground)
Labelling:	Binary, Motion vs. No-Motion

EXPERIMENTAL RESULTS AND QUANTITATIVE ANALYSIS

This section evaluates SD-threshold and STFT-Doppler detection against the empirical CSI data described in Experimental Sites, examining feature-level attenuation, environment-dependent detection performance, and per-zone confusion-matrix behaviour.

Feature-Level Attenuation

Fig. 1 and Fig. 2 plot peak Doppler energy and peak short-time standard deviation (SD) across the three NLoS zones (0.5–1.5 m, 1.5–2.5 m, 2.5–3.5 m) against Slow/Normal/Fast LoS baselines (mean ± SE bands). Doppler energy falls sharply into the first zone, from a Fast-LoS baseline near 3.3×10^5 to roughly 3.0×10^5, then plateaus around 2.6×10^5 from 1.5–2.5 m—a step-then-floor pattern rather than gradual decay. Its SE band never overlaps the Slow (≈ 10–14.5×10^5) or Normal (≈ 8.5–11.5×10^5) baselines at any distance, so separability from LoS movement holds throughout. Now SD tells the opposite story: it declines from ≈1.66 to ≈1.0 and its band closes directly onto the Fast-LoS baseline by the final zone, while staying clear of Normal (≈2.1–2.3) and Slow (≈3.3–3.9). This closing gap, not just the raw decline, is the operationally relevant result: Doppler energy stays statistically distinct from every LoS speed condition, while SD loses distinctiveness specifically against fast movement, which is the direct mechanism behind the SD-threshold false-negative failure reported in "Environment-Dependent Detection Performance" subsection.

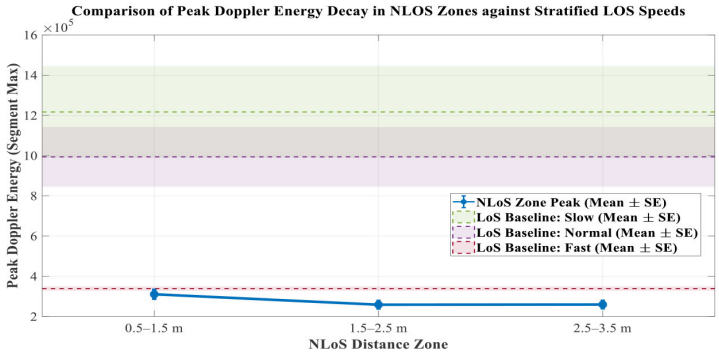


Figure 1: Transient peak Doppler energy (segment maximum) versus NLoS distance zone, LoS baseline and 0.5–1.5 m/1.5–2.5 m/2.5–3.5 m NLoS bins pooled across both sites. SE denotes the standard deviation error.

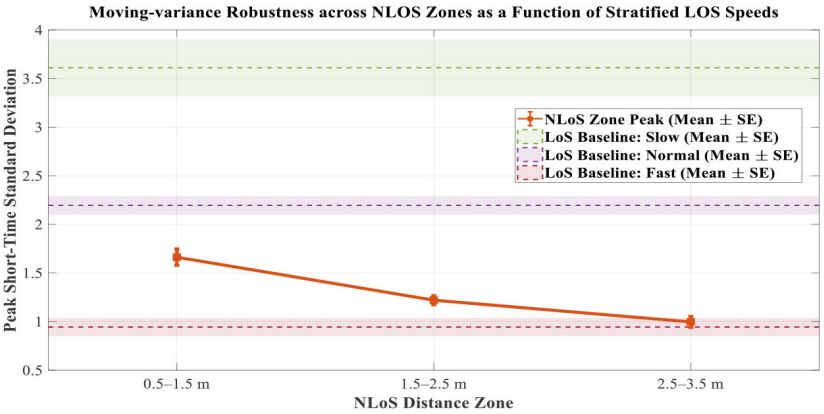


Figure 2: Transient peak short-time standard deviation versus NLoS distance zone, same binning as Fig. 1. SE denotes Standard deviation error.

Environment-Dependent Detection Performance

In the horticulture field (Fig. 3), SD-Threshold TPR declines monotonically from ≈0.63 (0.5–1.5 m) to ≈0.46 and ≈0.24 across successive zones, while STFT-Doppler holds a slightly less monotonic trajectory (≈0.54 → 0.41 → 0.37), yielding an F1 gap that widens from near-parity at 0.5–1.5 m to roughly 0.70 vs 0.54 at the farthest zone. On the other hand, in Nalanda Ground (Fig. 4), the divergence is far starker: SD-Threshold TPR falls from ≈0.20 to near zero beyond 1.5 m, driving F1 to zero, while STFT-Doppler sustains a non-monotonic trajectory with TPR of (≈0.62 → 0.49 → 0.61) and F1 of ≈0.66–0.77 across all three zones, with SE bands that never approach the SD-Threshold curve. This confirms the environment-dependent failure mode: SD-Threshold degrades gradually under vegetated scattering but collapses abruptly in open-field geometry, whereas STFT-Doppler remains the only detector with usable sensitivity at maximum NLoS offset in either environment.

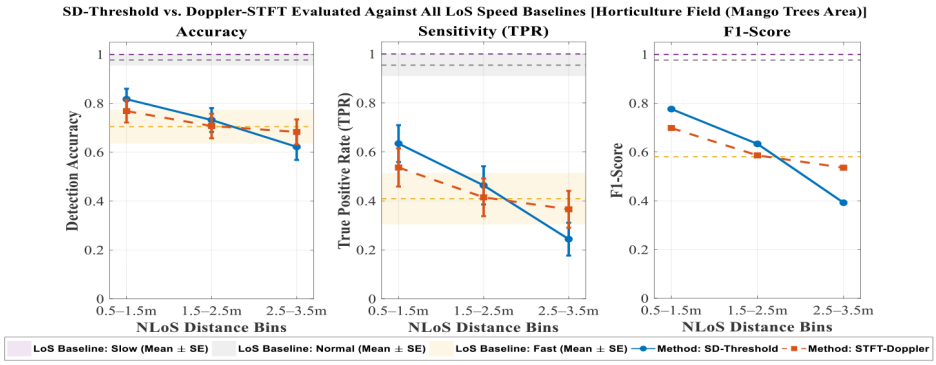


Figure 3: Performance of SD-Threshold and STFT-Doppler movement-detection methods across NLoS distance bins (0.5–3.5 m) in the horticulture field (mango trees area).

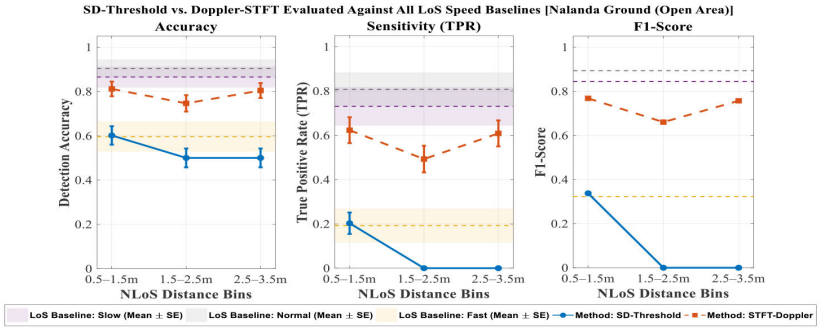


Figure 4: Performance of SD-Threshold and STFT-Doppler movement-detection methods across NLoS distance bins (0.5–3.5 m) in the nalanda ground (open-area) environment.

Confusion-Matrix Analysis

By using STFT-Doppler energy threshold in the horticulture field (Fig. 5), TPR on the "Move" class declines from 78.8% at avg. LoS to 53.7%, 41.5%, and 36.6% across the 0.5–1.5 m, 1.5–2.5 m, and 2.5–3.5 m NLoS zones, respectively, with no false positives on "No-Move" segments at any zone. The largest single-step degradation occurs between LoS and the 0.5–1.5 m zone, indicating that even minimal lateral offset under vegetated obstruction imposes substantial sensitivity loss; at 2.5–3.5 m, fewer than two in five motion events are detected.

In nalanda ground (Fig. 6), avg. LoS TPR is lower at baseline (57.7%) than in horticulture, but the NLoS trajectory is non-monotonic: 62.3% at 0.5–1.5 m, 49.3% at 1.5–2.5 m, and 60.9% at 2.5–3.5 m. We propose, as a hypothesis rather than a confirmed mechanism, that ground-reflected multipath at 5–7 m lateral offset intermittently reinforces motion-induced Doppler perturbations at specific geometries; testing this directly would require controlled reflector-position measurements, which we identify as future work. This pattern, distinct from the smooth horticulture degradation, supports reporting environment-specific results rather than pooled NLoS-distance curves.

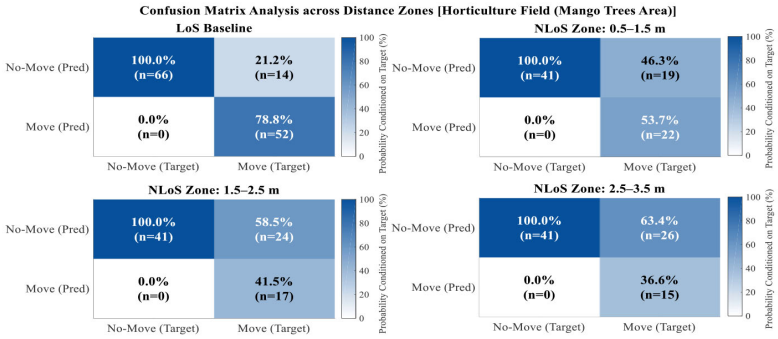


Figure 5: Normalized confusion matrices (using STFT-Doppler) for the horticulture field: (a) LoS baseline, (b) 0.5–1.5 m, (c) 1.5–2.5 m, (d) 2.5–3.5 m NLoS zones. N = 41 per NLoS zone.

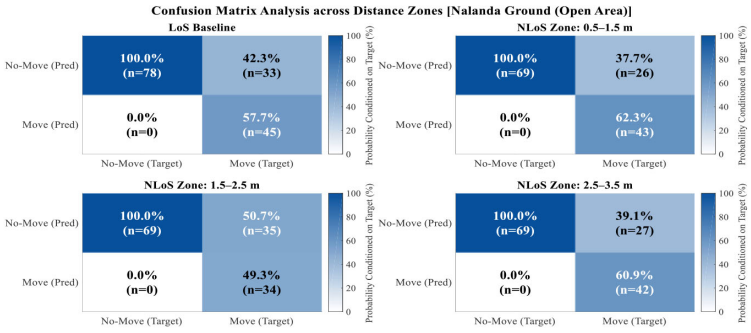


Figure 6: Normalized confusion matrices (using STFT-Doppler) for nalanda ground: (a) LoS baseline, (b) 0.5–1.5 m, (c) 1.5–2.5 m, (d) 2.5–3.5 m NLoS zones. N = 69 per NLoS zone.

CONCLUSION

This study presents a systematic experimental characterisation of CSI-based human motion detection under parameterised lateral NLoS offsets in outdoor agricultural and open-field environments, comparing SD-threshold and STFT-Doppler detection methods across 0.5–3.5 m lateral offsets using an ESP32-based acquisition platform.

The central result is environment-dependent. In the open-field Nalanda site, SD-threshold collapses (TPR = 0, F1 = 0) beyond 0.5–1.5 m NLoS offset, whereas STFT-Doppler sustains F1 scores of 0.66–0.77 across every distance tested. In the field of vegetated horticulture, both methods degrade with distance. Still, STFT-Doppler retains a consistent F1 advantage of 0.54 to 0.70 at the maximum offset tested. Both methods preserve perfect specificity (TNR = 100%) across all NLoS zones in both environments, so NLoS detection costs fall on missed detections rather than false alarms. This asymmetry carries a trust-calibration consequence for automated security monitoring: a system that raises no false alarms but silently stops detecting intrusion risks, sustaining operator confidence as its reliability collapses—a miss-dominant failure pattern recognised as damaging to appropriate reliance in automation (Lee and See, 2004; Hoff and Bashir, 2015). STFT-Doppler's sustained sensitivity is therefore justified on two grounds: stronger detection performance, and a lower risk of inducing unwarranted trust in a degraded system. Transient-feature analysis supports this distinction: peak Doppler energy falls to 50–90% of the LoS mean under NLoS offset via a step function rather than a gradual decay, while peak short-time SD declines near-monotonically toward the fast-LoS baseline, which underlies the loss of separability of the SD threshold. The 1.5–2.5 m zone marks the critical inflexion point where SD-threshold failure shifts from partial to complete in the open field.

These trials were limited to single-subject setups, fixed hardware, and specific weather conditions, so generalization across demographics, chipsets, and meteorological variation warrants caution. Within this scope, SD thresholds calibrated on LoS data should not be assumed transferable beyond 0.5–1.5 m NLoS offset without environment-specific recalibration, and STFT-Doppler should be the preferred detector for outdoor NLoS

deployment. Future work will extend this evaluation to multi-person scenarios, lightweight deep learning models, and long-term testing across varied macro-environments, providing a practical foundation for human-centred, privacy-preserving automation in agricultural security.

ACKNOWLEDGMENT

The authors wish to thank Mr Saride Satyasai Aravind Kumar for his assistance with data collection.

REFERENCES

Abdelnasser, H., Harras, K.A. and Youssef, M. (2015) 'WiGest demo: A ubiquitous WiFi-based gesture recognition system', *Proceedings - IEEE INFOCOM*, 2015-Augus, pp. 17–18. Available at: https://doi.org/10.1109/INFCOMW.2015.7179321.

Abuhoureyah, F.S., Wong, Y.C. and Mohd Isira, A.S. Bin (2024) 'WiFi-based human activity recognition through wall using deep learning', *Engineering Applications of Artificial Intelligence*, 127(PA), p. 107171. Available at: https://doi.org/10.1016/j.engappai.2023.107171.

Gringoli, F. *et al.* (2019) 'Free your CSI: A channel state information extraction platform for modern Wi-Fi chipsets', *Proceedings of the Annual International Conference on Mobile Computing and Networking, MOBICOM*, pp. 21–28. Available at: https://doi.org/10.1145/3349623.3355477.

Halperin, D. *et al.* (2011) 'Tool release', *ACM SIGCOMM Computer Communication Review*, 41(1), pp. 53–53. Available at: https://doi.org/10.1145/1925861.1925870.

Hoff, K.A. and Bashir, M. (2015) 'Trust in automation: Integrating empirical evidence on factors that influence trust', *Human Factors*, 57(3), pp. 407–434. Available at: https://doi.org/10.1177/0018720814547570.

Hu, Y. *et al.* (2022) 'DeFall: Environment-Independent Passive Fall Detection Using WiFi', *IEEE Internet of Things Journal*, 9(11), pp. 8515–8530. Available at: https://doi.org/10.1109/JIOT.2021.3116136.

ITU, I.T.U. (2016) 'Attenuation in vegetation', *ITU-R Recomm. 833-4* [Preprint].

Lee, J.D. and See, K.A. (2004) 'Trust in automation: Designing for appropriate reliance', *Human Factors*, 46(1), pp. 50–80. Available at: https://doi.org/10.1518/hfes.46.1.50_30392.

Li, J. *et al.* (2025) 'Non-line-of-sight identification from WiFi CSI using particle swarm optimization with multi-dimensional feature fusion', *Measurement: Journal of the International Measurement Confederation*, 242(PA), p. 115720. Available at: https://doi.org/10.1016/j.measurement.2024.115720.

Li, S. *et al.* (2020) 'Foreign object intrusion detection on metro track using commodity WiFi devices with the fast phase calibration algorithm', *Sensors (Switzerland)*, 20(12), pp. 1–26. Available at: https://doi.org/10.3390/s20123446.

Liu, X. *et al.* (2005) 'Quantifying drug-induced dyskinesias in the arms using digitised spiral-drawing tasks', *Journal of Neuroscience Methods*, 144(1), pp. 47–52. Available at: https://doi.org/10.1016/j.jneumeth.2004.10.005.

Olejniczak, A. *et al.* (2024) 'LOS and NLOS identification in real indoor environment using deep learning approach', *Digital Communications and Networks*, 10(5), pp. 1305–1312. Available at: https://doi.org/10.1016/j.dcan.2023.05.009.

Raja, P. and Riley, V. (1997) 'Humans and Automation: Use, Misuse, Disuse, Abuse', *HUMAN FACTORS*, 39(2), pp. 230–253.

Wang, W. *et al.* (2015) 'Understanding and modeling of WiFi signal based human activity recognition', *Proceedings of the Annual International Conference on Mobile Computing and Networking, MOBICOM*, 2015-Septe, pp. 65–76. Available at: https://doi.org/10.1145/2789168.2790093.

Wang, W. *et al.* (2017) 'Device-Free Human Activity Recognition Using Commercial WiFi Devices', *IEEE Journal on Selected Areas in Communications*, 35(5), pp. 1118–1131. Available at: https://doi.org/10.1109/JSAC.2017.2679658.

Wang, Y., Wu, K. and Ni, L.M. (2017) 'WiFall: Device-Free Fall Detection by Wireless Networks', *IEEE Transactions on Mobile Computing*, 16(2), pp. 581–594. Available at: https://doi.org/10.1109/TMC.2016.2557792.

Wei, Z. *et al.* (2025) 'Winal: Joint feature fusion and adversarial training for non line of sight WiFi localization', *Cluster Computing*, 28(12), pp. 1–16. Available at: https://doi.org/10.1007/s10586-025-05412-y.

Zhang, F. *et al.* (2018) 'WiSpeed: A Statistical Electromagnetic Approach for Device-Free Indoor Speed Estimation', *IEEE Internet of Things Journal*, 5(3), pp. 2163–2177. Available at: https://doi.org/10.1109/JIOT.2018.2826227.

Zhang, X. *et al.* (2022) 'Toward Reliable Non-Line-of-Sight Localization Using Multipath Reflections', *Proceedings of the ACM on Interactive, Mobile, Wearable and Ubiquitous Technologies*, 6(1), pp. 1–25. Available at: https://doi.org/10.1145/3517244.